# Grafting of polymer chains on the surface of carbon nanotubes via nitroxide radical coupling reaction

**Chengcheng Yang,[a] Monica Guenzi,[b] Francesca Cicogna,[a] Cristian Gambarotti,[b] Giovanni Filippone,[c] Calogero Pinzino,[a] Elisa Passaglia,[a] Nadka Tz. Dintcheva,[d] Sabrina Carroccio[e] and Serena Coiai[a]***

## INTRODUCTION

Today biodegradable alternatives to oil-based plastics are attracting great interest due to the growing need to use more sustainable materials. Aliphatic polyesters are considered economically competitive biodegradable plastics with good performances.[1,2] Among them, the synthetic poly(butylene succinate) (PBS) is a particularly interesting biodegradable polymer given that it is semicrystalline with thermoplastic processability similar to that of polyethylene and polypropylene, with good thermal and chemical resistance as well as strength and toughness values close to those of low density polyethylene.[3] However, for more widespread applications of PBS, its structural and functional properties need to be improved. For this purpose, one possible strategy envisages the introduction of a small amount of nanoparticles. A similar approach is receiving growing attention as it allows the performance of polymer matrices to be improved at reasonable cost without significantly altering their processability. Among the various kinds of nanoparticles, carbon nanotubes (CNTs) deserve particular attention owing to their unique thermal, mechanical, electrical and structural properties, which have considerably boosted their use as fillers for polymer nanocomposites in the last decade.[4,5] However, in order to fully take advantage of their characteristics, both a homogeneous dispersion throughout the polymer matrix and strong CNT – polymer interfacial interactions are necessary.[4] By contrast, the low compatibility between CNTs and polymer matrices often limits dispersion as well as the formation of well-organized architectures. Indeed, CNTs form clusters that look like very long bundles due to the high surface energy and stabilization by $\pi - \pi$ electron interactions among the tubes.

PBS/CNT nanocomposites with both single-walled CNTs (SWCNTs) and multi-walled CNTs (MWCNTs) have been prepared and characterized in the past. The melt-blending method[6–10] has generally been preferred, but solution blending has also been investigated[11,12] since under sonication a good dispersion of

* *Correspondence to: Serena Coiai, Istituto di Chimica dei Composti Organo Metallici (ICCOM), Consiglio Nazionale delle Ricerche, UOS Pisa, Via G. Moruzzi 1, 56124 Pisa, Italy. E-mail: serena.coiai@pi.iccom.cnr.it*

a *Istituto di Chimica dei Composti Organo Metallici (ICCOM), Consiglio Nazionale delle Ricerche, UOS Pisa, Via G. Moruzzi 1, 56124 Pisa, Italy*

b *Dipartimento di Chimica, Materiali e Ingegneria Chimica 'Giulio Natta', Politecnico di Milano, Politecnico di Milano, Piazza L. da Vinci 32, 20133 Milano, Italy*

c *Dipartimento di Ingegneria Chimica, dei Materiali e della Produzione Industriale, Università di Napoli Federico II, Piazzale V. Tecchio 80, 80125 Napoli, Italy*

d *Dipartimento di Ingegneria Civile, Ambientale, Aerospaziale, dei Materiali, Università di Palermo, Viale delle Scienze, Ed. 6, 90128 Palermo, Italy*

e *Istituto per i Polimeri, Compositi e Biomateriali (IPCB), Consiglio Nazionale delle Ricerche, UOS Catania, Via P. Gaifami 18, 95126 Catania, Italy*

the CNTs in solution can be obtained. The direct blending of unmodified CNTs shows the tendency of CNTs to form aggregates and to give a non-uniform dispersion in the polymer matrix with deleterious effects on the final properties. Indeed, the non-covalent method is generally not completely successful for preparing polymer/CNT nanocomposites except in the case of polar and aromatic polymers where strong polar and $\pi$-stacking interactions between the polymer chains and the CNT surface are established.[5]

In the case of PBS, better results in terms of morphology and final properties were achieved using functionalized CNTs, preferentially obtained by oxidation,[13] by the *N*,*N*′-dicyclohexylcarbodiimide (DCC) coupling method with alcohols or amines after oxidation[7,14,15] or by silanization modification reactions.[16] The use of functionalized CNTs allowed significant improvements in polymer – filler interactions and positive effects on the morphology and mechanical and thermal properties, as well as of the conductivity and crystallization behavior, to be achieved.[16]

The chemical bonding of polymer chains to CNTs is also known as a method able to greatly improve the dispersion of CNTs in the polymer phase as well as the interfacial strength and mechanical performance.[17] Indeed, the grafting of polymer chains on the sidewalls of CNTs promotes the formation of an immobilized interfacial layer, which improves the dispersion in polymer matrices and in organic solvents. Moreover, the grafting of the CNTs to the polymer may be considered as a solution for the risk associated with the migration and release of nanostructures during the production, use, end of life and recycling of these nanocomposite materials.

Generally, polymer-grafted CNTs are prepared either by 'grafting from' or by 'grafting to' methodologies. The 'grafting from' method starts with the immobilization of an initiator on the CNT surface followed by *in situ* polymerization with the generation of grafted polymer brushes.[18] On the other hand, the 'grafting to' method is based on the grafting of preformed polymer chains by chemical reaction (generally amidation or esterification reactions) with modified CNTs. As an example of 'grafting from' of a biodegradable aliphatic polyester on MWCNTs, poly(lactic acid) (PLA) chains were covalently grafted on the surfaces of MWCNTs by a two-step process involving first the grafting of the $SnOct_2$ initiator on MWCNTs functionalized with hydroxyl groups, followed by the surface initiated ring-opening metathesis polymerization *in situ* of L-lactic acid.[19] Similarly, PLA was covalently grafted in one-pot by *in situ* polycondensation of L-lactic acid in the presence of a catalyst and of MWCNTs functionalized with carboxylic groups.[20] In the last case it is believed that the functional moieties on the MWCNTs take part in the polycondensation of L-lactic acid; therefore the method involves both the 'grafting to' and the 'grafting from' approach. In the case of PBS, Tan *et al.*[16] reported a 'grafting to' method of PBS on the sidewalls of SWCNTs. The surface of SWCNTs was first modified by a silanization reaction using an aminosilane as modifying agent, thus introducing ethoxyl groups on the surface of the SWCNTs. Later, the ethoxyl groups reacted with the carboxylic acid terminal groups of PBS by a hydrolysis condensation reaction during the physical blending, thus creating a covalent bond between the two phases. Some advantages were achieved by this method. In particular, the procedure allowed the crystallization of the PBS in the nanocomposites to be enhanced due to the heterogeneous nucleation effect. Moreover the covalent bonding forced the SWCNTs to be better dispersed in PBS, and nanocomposites with high tensile strength and low loss factor were obtained.

In this work, an alternative method for grafting aliphatic polyesters to the sidewalls of MWCNTs is proposed. In view of the experience of our group in the grafting of functional TEMPO (2,2,6,6-tetramethyl-1-piperidinyloxy) molecules to different classes of polymers, such as polyolefins[21,22] and aliphatic biodegradable polyesters (i.e. PBS and PLA),[23] via the nitroxide radical coupling (NRC) reaction, here we demonstrate the possibility of exploiting the NRC reaction to graft PBS chains onto MWCNTs with the purpose of producing nanocomposites with improved dispersion and with the nanotubes embedded/immobilized in the polymer matrix. An advantage of this method based on a radical-induced reaction is that the grafting of the nitroxide moieties occurs without involving severe degradation of the polymer matrix. Accordingly, the main properties of the matrix remain unchanged after the process. Moreover, in contrast with the literature,[24] a new and highly efficient covalent attachment of nitroxide radicals on the sidewalls of MWCNTs was provided here by click chemistry.[25,26] Alkyne-containing nitroxide radicals were grafted on an azide functional MWCNT surface to obtain MWCNTs-*g*-TEMPO. Afterwards, PBS macroradicals were generated via peroxide in solution and trapped by the NRC reaction with MWCNTs-*g*-TEMPO. Electron paramagnetic resonance (EPR) spectroscopy was exploited to verify the successful functionalization of MWCNTs and to confirm the grafting of the polymer chains. Then, the thermal and rheological properties of the composite were investigated using as reference material a blank sample obtained by simple physical mixing of PBS and functional MWCNTs. The preliminary results indicate a better dispersion of the grafted nanotubes, revealing the NRC reaction as an effective tool for the covalent functionalization of nanoparticles.

## EXPERIMENTAL

### Materials

PBS Bionolle 1001, supplied by Showa HighPolymer Co. Ltd (Tokyo, Japan), melt flow index (2.16 kg, 190 °C) 1.5 g $(10\ min)^{-1}$ (from the technical data sheet), was used as the polymer matrix. PBS was dried in a vacuum oven at 80 °C for 18 h before use. Glutaric anhydride (95%), 4-hydroxy-TEMPO (97%), propargyl bromide (*ca* 80% in toluene), sodium hydride (60% dispersion in mineral oil), DCC (≥99.0%), 3-bromo-1-propanol (97%), sodium azide (≥99.0%) and copper(I) iodide (98%) were purchased from Sigma-Aldrich (Milano, Italy) and used without further purification. 1,4-dioxane from Carlo Erba (Milano, Italy) (RPE, 99%) was distilled over Na and stored over activated molecular sieves before use. Tetrahydrofuran (Sigma-Aldrich, anhydrous with 250 ppm of 2,6-di-tert-butyl-4-hydroxytoluene (BHT) as inhibitor, ≥99.5%) and dimethylformamide (Sigma-Aldrich, anhydrous, ≥99.8%) were used as received without further distillation/dehydration. Chloroform (Carlo Erba, RPE grade), chloroform (Sigma-Aldrich, HPLC grade, ≥99.8%, amylene stabilized), methanol (Sigma-Aldrich) and 2-propanol (Sigma-Aldrich) were used without further purification. Dibenzoyl peroxide (BPO) (Sigma-Aldrich) was used as received.

### Preparation of TEMPO functionalized MWCNTs

MWCNTs were prepared by the typical chemical vapor deposition protocol using ethylene as carbon source.[27] The purification was performed with 50% aqueous sulfuric acid, obtaining carbon nanotubes with outer diameter ranging between 15 and 25 nm, inner diameter in the range 4 – 8 nm, length 10 – 20 μm and purity

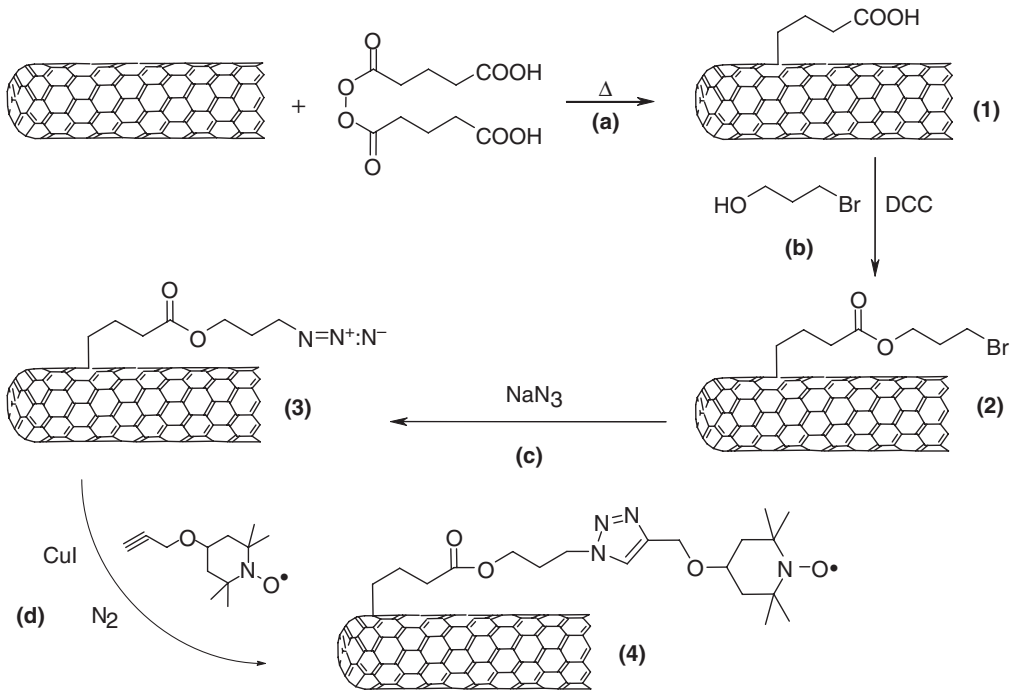


**Scheme 1.** Preparation of MWCNTs-*g*-TEMPO.

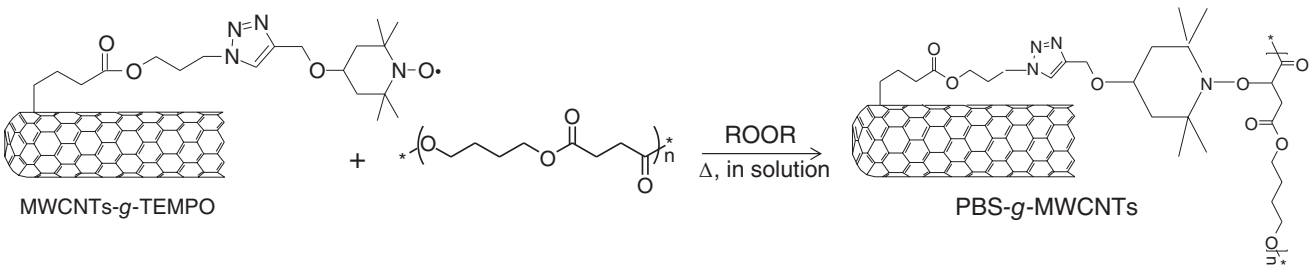


**Scheme 2.** NRC reaction between MWCNTs-*g*-TEMPO and PBS.

>98 wt%. The MWCNTs obtained were further functionalized by *in situ* thermal degradation of glutaryl peroxide (Scheme 1, step (a)) (see Doc. S1 for experimental details), which was previously prepared from glutaric anhydride (Scheme S1) following the procedure reported in the literature.[28,29]

The MWCNTs **1** were analyzed by X-ray photoelectron spectroscopy (Fig. S1), which showed an oxygen atom abundance of about 3.1%, evidenced by the signals at 287.36 eV and 289.340 eV of C(1 s) (Fig. S1, top) and by the signals at 531.87 eV and 533.35 eV of O(1 s) (Fig. S1, bottom). The 0.6% of aluminium was derived from the residual catalyst utilized in the preparation of the nanotubes. The acidic functions on the surface of the MWCNTs **1** were also titrated (see Doc. S1), obtaining, in agreement with the X-ray photoelectron spectroscopy analysis, a mass abundance of carboxylic groups of between 3% and 4%.

Steps (b) and (c) were performed without any characterization of the intermediates **2** and **3**. MWCNTs **1** were esterified with 3-bromo-propanol in the presence of DCC to the corresponding bromo derivative **2** (Scheme 1, step (b)) (see Doc. S1); then the Br was substituted by the azido group (Scheme 1, step (c)) (Doc. S1), obtaining the azido derivative **3**. The 'click' coupling between **3** and 4-propargyl-TEMPO, previously prepared following the procedure reported in the literature[30] (Scheme S2), provided the target MWCNTs-*g*-TEMPO **4** (Scheme 1, step (d)) (Doc. S1).[31,32]

## Preparation of PBS composites containing MWCNTs-*g*-TEMPO

### *Preparation of PBS covalently grafted to MWCNTs-g-TEMPO (PBS-g-*MWCNTs)

MWCNTs-*g*-TEMPO (25 mg) was dispersed into 1,4-dioxane (60 mL) under nitrogen by water bath ultrasound sonication at 50 °C for 3 h. PBS (2.5 g) was then added into the MWCNT dispersion under sonication at 65 °C for 1 h until the polymer was completely dissolved. After that, the dispersion was heated to 90 °C out of the sonication bath, and 0.5 mL of a $3.5 \times 10^{-6}$ mol $L^{-1}$ solution of BPO in 1,4-dioxane (0.5 mL) was added dropwise. The reaction was carried out under a nitrogen atmosphere at 90 °C for 2.5 h with magnetic stirring (Scheme 2).

After the reaction, the dispersion was cooled and poured into methanol (250 mL). The product was washed with methanol at room temperature for 5 h to remove low molecular weight compounds deriving from the peroxide decomposition. A solid grey powder was collected, washed again with methanol for further purification and finally vacuum dried. To clearly identify the presence of the grafted PBS phase, 46 mg of the composite were dispersed in 3 mL of chloroform under magnetic stirring for 1 h and

then the dispersion was centrifuged at 6000 rpm for 10 min to promote phase separation. This procedure was repeated until the PBS disappeared from the soluble fraction, as checked by collecting the Fourier transform IR (FTIR) spectrum of the washing solvent. The final residue was collected, dried and analyzed by attenuated total reflectance (ATR) FTIR.

*Preparation of the physical blend between PBS and MWCNTs-g-TEMPO (MWCNTs/PBS)*

A reference composite was prepared by physical mixing of PBS and MWCNTs-*g*-TEMPO. With the exception of the addition of peroxide, the procedure adopted for the preparation of the PBS-*g*-MWCNTs sample was followed.

**Characterization**

Infrared spectra were recorded using a PerkinElmer Spectrum 100 FTIR spectrometer equipped with a universal ATR accessory and a TGS detector. The ATR-FTIR spectra of MWCNTs-*g*-TEMPO, PBS and the chloroform-insoluble fraction of the PBS-*g*-MWCNTs were collected from powders.

The number-average molecular weight ($M_n$) and weight-average molecular weight ($M_w$) as well as the dispersity ($M_w/M_n$) of the samples were determined using SEC, Agilent Technologies 1200 Series. The instrument was equipped with an Agilent degasser, an isocratic HPLC pump, an Agilent refractive index detector and two PLgel 5 μm MiniMIX-D columns conditioned at 35 °C. Chloroform was used as the mobile phase at a flow rate of 0.3 mL min$^{-1}$. The system was calibrated with polystyrene standards in the range from 500 to $3 \times 10^5$ g mol$^{-1}$. Samples were dissolved/dispersed in chloroform (2 mg mL$^{-1}$) and filtered through a 0.20 μm syringe filter three times before analysis. $M_n$ and $M_w$ were determined using Agilent ChemStation Software.

TGA was performed using a Q5000 TGA apparatus (TA Instruments). The PBS and the composite samples were first heated at 10 °C min$^{-1}$ from room temperature up to 650 °C in gaseous nitrogen and were held at 650 °C for 5 min to verify the completion of the thermal degradation processes. MWCNTs-*g*-TEMPO was also characterized from room temperature to 700 °C under a nitrogen flow at a heating rate of 10 °C min$^{-1}$; the residue at 650 °C was about 17 wt% (Fig. S2).

DSC analyses were carried out on 9–11 mg of samples by using a Seiko Exstar SII DSC 7020 instrument. The glass transition and melting temperatures were evaluated from the second heating curve of three subsequent heating – cooling scans performed from −70 to 130 °C at a heating rate of 10 °C min$^{-1}$ and a cooling rate of 50 °C min$^{-1}$ under a nitrogen purge flux. The crystallization temperature of the samples was registered by the cooling scan.

X-band EPR spectra were obtained with a Varian E112 spectrometer equipped with a Varian E257 temperature control unit. The EPR spectrometer was interfaced to an IPC 610/P566C industrial grade Advantech computer by means of a data acquisition system. This unit consists of an acquisition board capable of acquiring up to 500 000 12-bit samples per second[33] and a software package specially designed for EPR experiments.[34] The EPR spectra of 4-propargiloxy-TEMPO and MWCNTs-*g*-TEMPO were obtained at room temperature by analyzing a solution of 4-propargiloxy-TEMPO in 2-propanol (1.15 mg mL$^{-1}$) and the stable portion of a sonicated dispersion of MWCNTs-*g*-TEMPO in 2-propanol (0.43 mg mL$^{-1}$), respectively. An EPR spectrum of the solid MWCNTs-*g*-TEMPO (3.5 mg) was also collected at room temperature. Finally, EPR spectra of PBS-*g*-MWCNTs were collected by placing a small amount of the sample (7.5 mg) in a quartz tube (internal diameter 2 mm) and gradually increasing the temperature.

TEM analyses were carried out using a JEOL JEM-2100 high resolution transmission electron microscope at the Centro Grandi Apparecchiature – UninetLab, University of Palermo. The analyses were carried out on ultrathin slides (films) with a thickness of about 100 nm. Ultrathin films of the samples were prepared via cutting from films of the composites embedded in an epoxy resin with a Leica Ultramicrotome EM-UC6. The ultrathin slides of the samples were mounted on lacey carbon films on 300 mesh copper grids and then observed with the JEOL JEM-2100 under an accelerated voltage of 200 kV.

Rheological analyses were carried out using a stress-controlled rotational rheometer (AR-G2 by TA Instruments) in parallel plate geometry (plate diameter 25 mm). The specimens were disks (diameter 25 mm, thickness *ca* 1 mm) prepared by means of a hydraulic press (LP20-B, Labtech Engineering). The materials were compacted at $T = 125$ °C under a pressure $P \approx 150$ bar for 2 min, and then the pressure was removed and the samples were cooled to room temperature at *ca* 30 °C min$^{-1}$. The disks were dried overnight at 40 °C, and then oscillatory experiments were performed at $T = 160$ °C in a nitrogen atmosphere. In particular, the samples were subjected to frequency scans from $\omega = 10^2$ down to $10^{-1}$ rad s$^{-1}$, and the elastic ($G'$) and viscous ($G''$) shear moduli were recorded. The tests were carried out at a strain amplitude low enough to be in the linear regime, which was previously estimated by means of strain sweep experiments. Time scan experiments at $\omega = 10^{-1}$ rad s$^{-1}$ were also performed to ascertain the time stability of the samples.

## RESULTS AND DISCUSSION

**TEMPO functionalized MWCNTs**

EPR spectroscopy was used to confirm the covalent grafting of the TEMPO moieties on the MWCNTs. The EPR spectrum of 4-propargiloxy-TEMPO in 2-propanol at known concentration was acquired first (Fig. 1(a)) and compared with that of a stable sonicated dispersion of the MWCNTs-*g*-TEMPO in the same solvent (Fig. 1(b)).

The X-band EPR spectrum of 4-propargiloxy-TEMPO radicals in 2-propanol solution shows a symmetric three-line signal typical of nitroxide species, which is due to the hyperfine coupling of the nitroxide to $^{14}$N nuclear spin.[31] The number of spins calculated from the spectrum corresponds to $3.29 \times 10^{17}$, which is in agreement with the molecules added in the EPR tube. The fitting curve is also very close to the experimental curve. Moreover, the rotational correlation time $\tau$ was calculated by line-shape analysis of the spectrum. This parameter indicates the degree of motion of nitroxide in the solution, which was equal to 42 ps. The EPR spectrum of MWCNTs-*g*-TEMPO in 2-propanol suspension (a stable portion of the precursor suspension was analyzed, see Experimental section for details of preparation.) showed an asymmetric three-line signal due to the nitroxide grafted on MWCNTs and entrapped in this rigid phase. A fit of the spectrum was carried out to obtain the rotational correlation time $\tau = 0.52$ ns. This longer correlation time of nitroxide moieties grafted on MWCNTs is probably due to the confinement of the nitroxide motions.[31] Such a result proves the successful covalent attachment of nitroxide radicals on the sidewalls of MWCNTs. Since the analysis was carried out only on a stable portion of the suspension, we were not able

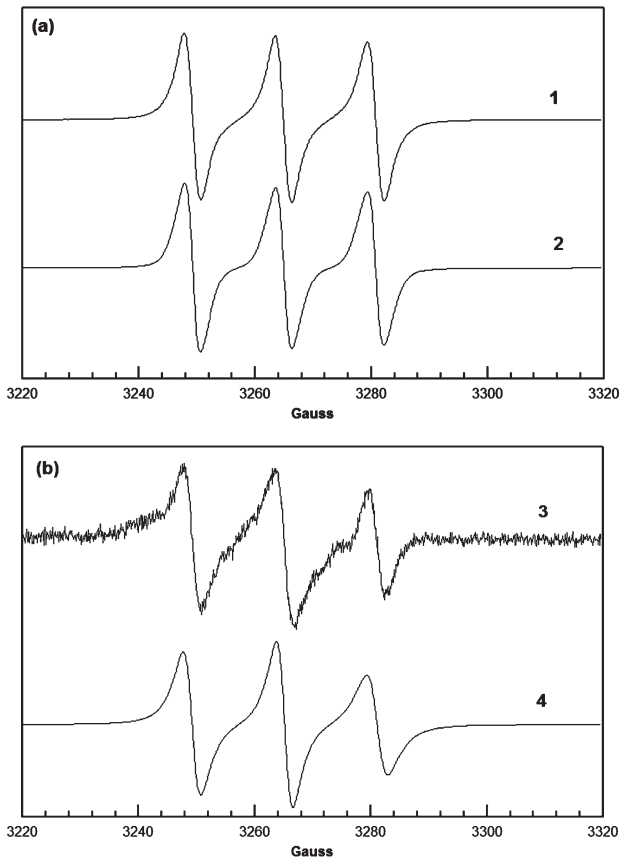


**Figure 1.** X-band EPR spectra of (a) 4-propargyloxy-TEMPO radicals in 2-propanol solution and (b) MWCNTs-*g*-TEMPO in 2-propanol suspension at 25 °C. Curves 1 and 3, experimental curves; curves 2 and 4, fitting curves.

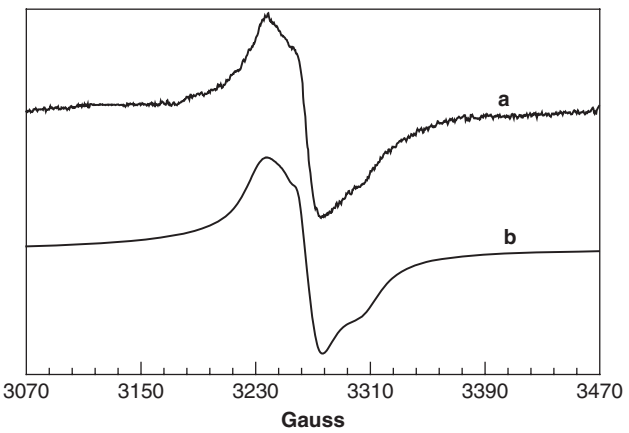


**Figure 2.** X-band EPR spectra of solid MWCNTs-*g*-TEMPO at 25 °C: curve a, experimental curve; curve b, fitting curve.

to associate the number of spins calculated with the amount of MWCNTs-*g*-TEMPO really suspended. Therefore, the EPR spectrum of the solid MWCNTs-*g*-TEMPO was collected to estimate the number of grafted functional moieties (Fig. 2).

By considering the amount of MWCNTs-*g*-TEMPO and the number of spins calculated from the EPR spectrum corresponding to $1.51 \times 10^{17}$, the quantity of functional grafted groups on the MWCNTs was estimated to be 2.7 wt%, corresponding to 0.072 mmol of TEMPO moieties per gram of nanotubes.

## 'GRAFTING TO' OF PBS ON MWCNTS VIA THE NRC REACTION

The NRC reaction between MWCNTs-*g*-TEMPO and PBS was carried out at 90 °C in 1,4-dioxane using BPO as radical initiator. This temperature was selected to ensure the complete dissolution of PBS in the solvent and to fit the thermal decomposition of BPO within the reaction time. Ultrasound sonication was also applied to promote an appropriate dispersion of MWCNTs-*g*-TEMPO. The amount of peroxide was chosen on the basis of the number of grafted nitroxide moieties on the sidewall of the nanotubes, as previously determined.[23] The quantity of peroxide was estimated taking into account the half-life of the peroxide at the working temperature, knowing that part of the peroxide is lost in degradation reactions during its thermal decomposition and considering that the concentration of macroradicals needs to be well weighted to control polyester side reactions promoting the macroradical – nitroxide coupling reaction. Since the nominal amount of MWCNTs-*g*-TEMPO with respect to PBS is 1 wt%, the concentration of BPO was chosen to be equal to the moles of grafted TEMPO moieties. Accordingly the amount of active primary radicals is the same as the nitroxide radicals (Table 1).

With the aim of providing a composite without covalent bonds between the polymer phase and nanotubes, a physical mixture containing PBS and MWCNTs-*g*-TEMPO (labeled MWCNTs/PBS), with polymer and filler content reproducing the PBS-*g*-MWCNTs sample, was prepared.

The purified PBS-*g*-MWCNTs was characterized by EPR analysis with the aim of providing direct evidence of the grafting. The powdered sample was introduced into the EPR cavity and spectra were registered at different temperatures. At the beginning of the experiment (at 40 °C), the spectrum showed only a weak and unstructured signal, which may be due to TEMPO moieties that did not take part in the NRC reaction with PBS macroradicals or that can be present in the medium owing to the nitroxide – alkoxyamine equilibrium.[35–37] As the temperature was increased to 120 °C, the same signal appeared as an asymmetric three-line signal. After a period of 5 min at 180 °C the system was cooled to 120 °C and the spectrum was recorded again. A significant increase of the integral was noticed with respect to the previous one probably due to the nitroxide radicals formed by homolytic cleavage carried out at 180 °C of the C – ON bond between the PBS and functional MWCNTs (Fig. 3). Due to the very high reactivity of carbon-centered radicals, which at high temperatures can give rise to recombination reactions, the nitroxide radicals formed by homolytic cleavage remain free at 120 °C thus increasing the total area of the signal. The area of this signal corresponds to $4.09 \times 10^{14}$ spins, which represents about 10% – 12% of the moles of TEMPO groups of this composite. Accordingly, full cleavage of the C – ON bonds was not reached in these conditions, as previously evidenced.[23]

To further confirm the grafting of the PBS chains on the MWCNTs, the PBS-*g*-MWCNTs sample was repeatedly washed with chloroform and then centrifuged to remove the non-grafted polymer. After drying, the residue was characterized by FTIR and its spectrum was compared with those of MWCNTs-*g*-TEMPO and neat PBS (Fig. 4), respectively.

The ATR-FTIR spectrum of the MWCNTs-*g*-TEMPO shows a very weak signal at about 1710 – 1715 $cm^{-1}$ and weak stretching signals in the CH stretching region that confirm the successful grafting by click chemistry of the functional TEMPO unit bearing an ester functionality, as also evidenced by EPR results. The spectrum of the

**Table 1.** Feed composition and molecular weight of PBS-*g*-MWCNTs and MWCNTs/PBS blank

| Sample name | Feed composition | | Molecular weights and distribution[a] | | |
|---|---|---|---|---|---|
| | BPO[b](mol%) | MWCNTs-*g*-TEMPO[c] (wt%) | $M_n$ (kDa) | $M_w$ (kDa) | $M_w/M_n$ |
| PBS[c] | – | – | $17.3 \pm 0.5$ | $42.7 \pm 1.1$ | $2.47 \pm 0.07$ |
| PBS-*g*-MWCNTs | 0.012 | 1 | $17.8 \pm 0.4$ | $44.5 \pm 0.7$ | $2.50 \pm 0.08$ |
| MWCNTs/PBS | – | 1 | $16.9 \pm 0.7$ | $43.8 \pm 1.1$ | $2.60 \pm 0.14$ |

[a] $M_n$, $M_w$ and $M_w/M_n$ are mean values of three measurements ± standard deviation.
[b] The moles of BPO are equal to the moles of TEMPO units grafted on the MWCNTs. The mol% of BPO was calculated with respect to the moles of repeating monomeric units of PBS. [c]The MWCNTs-*g*-TEMPO percentage was calculated with respect to PBS.
[c] PBS was dissolved in dioxane and heated at 90 °C for 2.5 h.

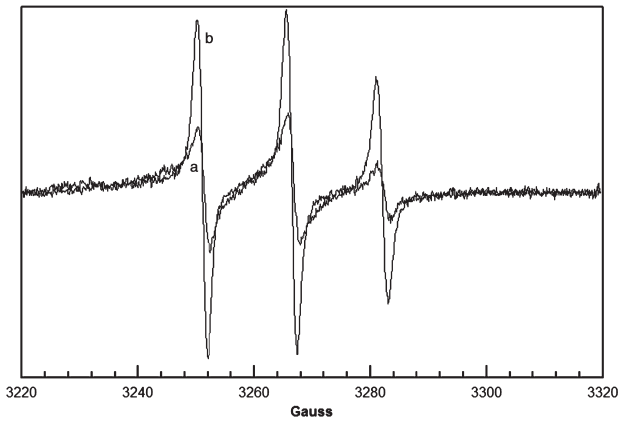


**Figure 3.** EPR spectra of PBS-*g*-MWCNTs registered at 120 °C (curve a) and at 120 °C after 5 min at 180 °C (curve b).

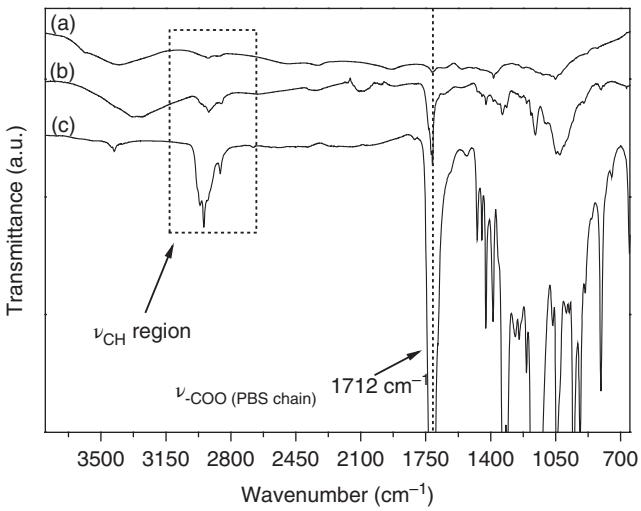


**Figure 4.** ATR-FTIR spectra of MWCNTs-*g*-TEMPO (curve (a)), residue of PBS-*g*-MWCNTs after chloroform extraction (curve (b)) and PBS (curve (c)).

residue to the chloroform extraction clearly evidences the –COO stretching signal of the PBS ester units at 1712 cm$^{-1}$ and signals probably due to stretching vibrational motions of $CH_2$ can be noticed in the CH stretching region, both confirming the polymer chain grafting.

The physical mixture MWCNTs/PBS was subjected to the same extraction procedure. As expected, in the case of the blank the ATR-FTIR analysis did not show the presence of PBS, which was completely removed by the extraction procedure.

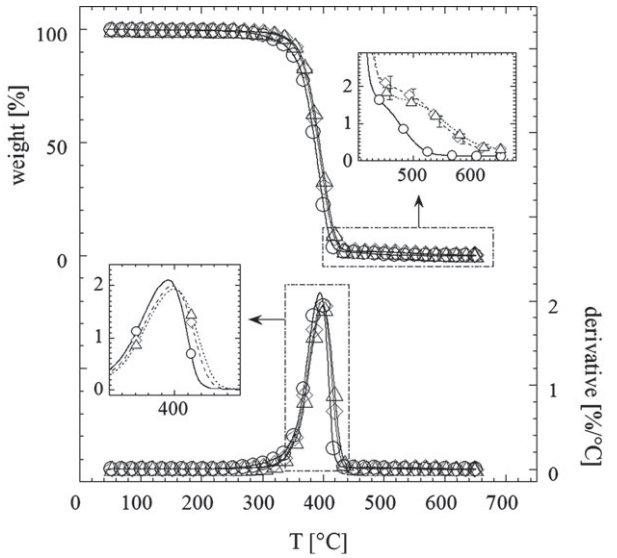


**Figure 5.** TGA (top, left axis) and DTGA (bottom, right axis) curves for neat PBS (circles), MWCNTs/PBS (diamonds) and PBS-*g*-MWCNTs (triangles). The error bars in the upper inset are the standard deviations over three independent tests.

The molecular weight data of all the PBS samples (Table 1) were determined by SEC analysis with the aim of verifying if the primary radicals generated by the peroxide decomposition had modified the molecular weight of the matrix. Indeed, the free radical functionalization of the polymer matrix is usually accompanied by side reactions that can cause a variation of the molecular weight of the polymer altering the mechanical, thermal and rheological properties of the polymer matrix. SEC data (Table 1) showed that the addition of MWCNTs-*g*-TEMPO in combination with the peroxide did not cause a change in the solubility of the polymer, and both $M_n$ and $M_w$ were comparable to those of PBS solubilized in dioxane and heated at 90 °C and those of the blank reference mixture. Accordingly, by the NRC reaction it is possible to control radical-induced side reactions,[21–23] such as the coupling reaction between the PBS macroradicals, thus avoiding the possible branching/crosslinking of the matrix[23] and preserving the macromolecular structure of the pure polymer.

### Effect of grafting on the structure and properties of PBS nanocomposites

The grafting of PBS molecules on the surface of the nanotubes is expected to favor their dispersion and degree of interaction with the host PBS. To prove this, preliminary investigations were

**Table 2.** TGA data of neat PBS, MWCNTs/PBS and PBS-*g*-MWCNTs

| | TGA data | | |
|---|---|---|---|
| Sample | $T_{d10\%}$ (°C) | $T_{peak}$ (°C) | Residue (wt%) |
| PBS | 346.5 ± 0.4 | 394.2 ± 0.6 | 0.12 ± 0.04 |
| MWCNTs/PBS | 356.5 ± 0.6 | 397.2 ± 0.8 | 0.33 ± 0.02 |
| PBS-*g*-MWCNTs | 359.4 ± 0.4 | 398.8 ± 0.7 | 0.35 ± 0.05 |

$T_{d10\%}$ is the thermal decomposition temperature at 10 wt% weight loss; $T_{peak}$ is the temperature at the maximum degradation rate; the residue has been evaluated at 650 °C. TGA analyses were repeated three times per sample and the standard deviation was calculated.

performed taking the simply mixed MWCNTs/PBS sample as reference. First, TGA was performed to check the thermal stability of the two composites and to confirm that they contain the same amount of nanoparticles. The results are reported in Fig. 5 and Table 2 together with the data of pure PBS.

All the samples share a predominant thermal degradation process in the temperature range 350–450 °C. An increment of about 10–15 °C of the thermal decomposition temperature at 10 wt% weight loss ($T_{d10\%}$) is noticed in both filled samples. This is expected, being due to a shielding effect of the nanotubes that inhibits the elimination of volatile byproducts, hindering the flux of degradation product and, as a consequence, delaying the onset of degradation.[38,39] Regarding the residues at $T = 650$ °C, the collected results confirm that the two nanocomposites contain exactly the same actual amount of filler. The latter is lower than the nominal content of CNTs added during the sample preparation probably due to some material loss in the course of the grafting or mixing procedures.

The dispersion level of the nanotubes in the filled samples was investigated via TEM and rheological analyses. Two representative micrographs of the PBS-*g*-MWCNTs and MWCNTs/PBS samples are shown in Fig. 6.

The coexistence of individual nanotubes and some small bundles is noticed in both cases. However, the low contrast typical of carbon-based structures dispersed in polymer matrices, as well as the narrowness of the portion of sample probed by TEM analyses, make it difficult to draw conclusions about the overall state of the dispersion filler and, even less, the interfacial features. Further information on this matter was collected through rheological analyses, which allow macroscopic samples to be probed. The viscoelastic shear moduli of the nanocomposites and pure PBS are shown in Fig. 7(a).

The pure polymer exhibits pseudo-Newtonian behavior ($G'' >> G'$, $G'' \sim \omega^1$, $G' \sim \omega^2$). In contrast, both filled samples are characterized by marked elastic connotation ($G' > G''$) and weak $\omega$ dependence at low frequency. These are typical rheological fingerprints of polymer nanocomposites above the filler percolation threshold. The viscoelasticity of this class of materials is essentially determined by the nanotube network embedded in the host polymer, which arrests the relaxation dynamics imparting solid-like behavior to the sample. In particular, the low-frequency plateau of the elastic modulus ($G'_0$) is a measure of the network elasticity. At a fixed composition, the latter essentially depends on the space arrangement of the network building blocks, i.e. the single nanotubes, as well as on the quality of stress transfer across the polymer – particle interface: the better the filler dispersion and degree of interaction with the matrix, the higher the value of $G'_0$.

The viscous moduli of the two filled samples are exactly the same. This is not surprising, as the $G''$ of the polymer nanocomposites is essentially governed by the polymer matrix, which is the same in the two samples. Clear differences instead emerge when comparing the elastic moduli. In particular, $G'_0$ of the PBS-*g*-MWCNTs sample is almost twice that of the MWCNTs/PBS sample, or alternatively the strength of the network based on grafted nanotubes is twice that of the network formed by particles simply mixed with the polymer. This means that the PBS-*g*-MWCNTs sample can bear double the shear stress of the MWCNTs/PBS sample without flowing. This can be clearly seen in Fig. 7(b), where the complex viscosity ($\eta^*$) is reported as a function of the oscillatory shear stress $\tau$. The typical behavior of a Bingham fluid is observed: $\eta^*$ diverges when approaching from above a critical shear stress $\tau_c$, which marks the transition from solid-like ($\tau < \tau_c$) to liquid-like ($\tau > \tau_c$) behavior. It is clear from Fig. 7(b) that the $\tau_c$ of the PBS-*g*-MWCNTs sample is about double that of the MWCNTs/PBS sample. This result is in agreement with the occurrence of stronger interactions between PBS and MWCNTs agreeing with the grafting of the polymer chains on the nanotubes.

The crystallization and melting behaviors of different samples were investigated by DSC. The thermograms collected from both

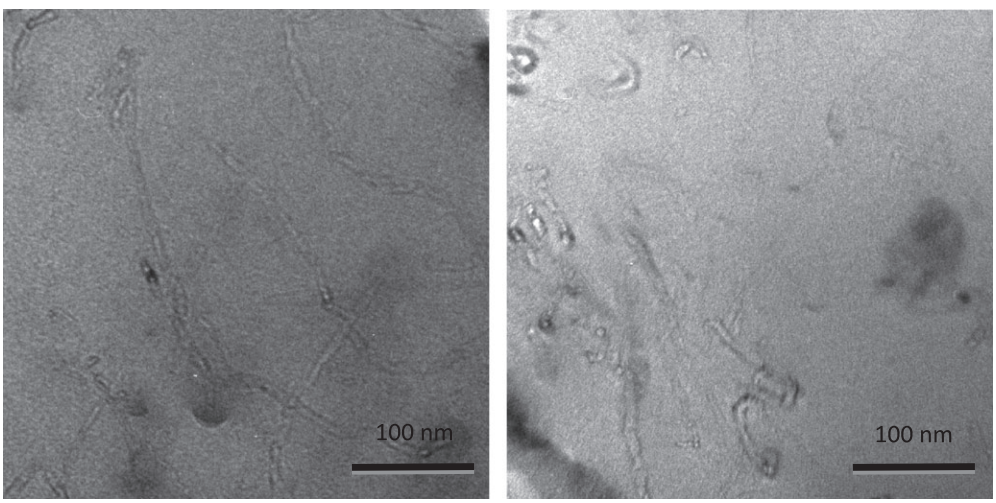


**Figure 6.** TEM images of PBS-*g*-MWCNTs (left) and MWCNTs/PBS (right).

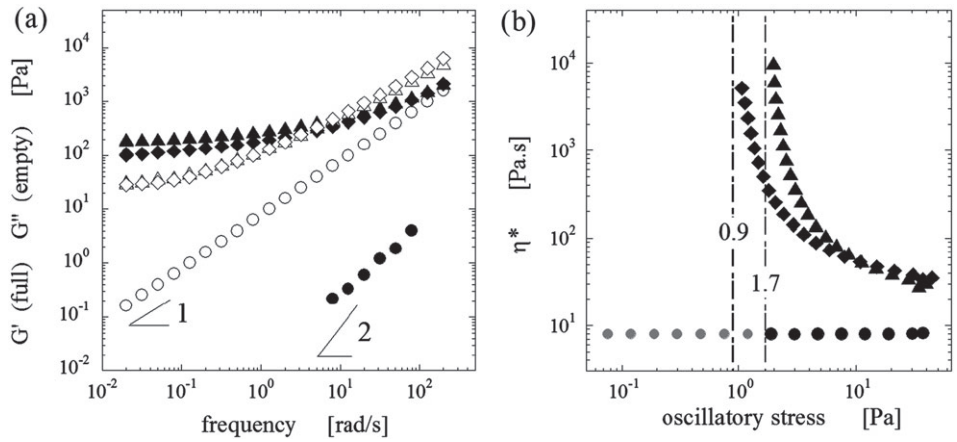


**Figure 7.** Frequency dependence of the shear moduli (a) and complex viscosity as a function of the oscillatory shear stress (b) for pure PBS (circles), MWCNTs/PBS (diamonds) and PBS-*g*-MWCNTs (triangles).

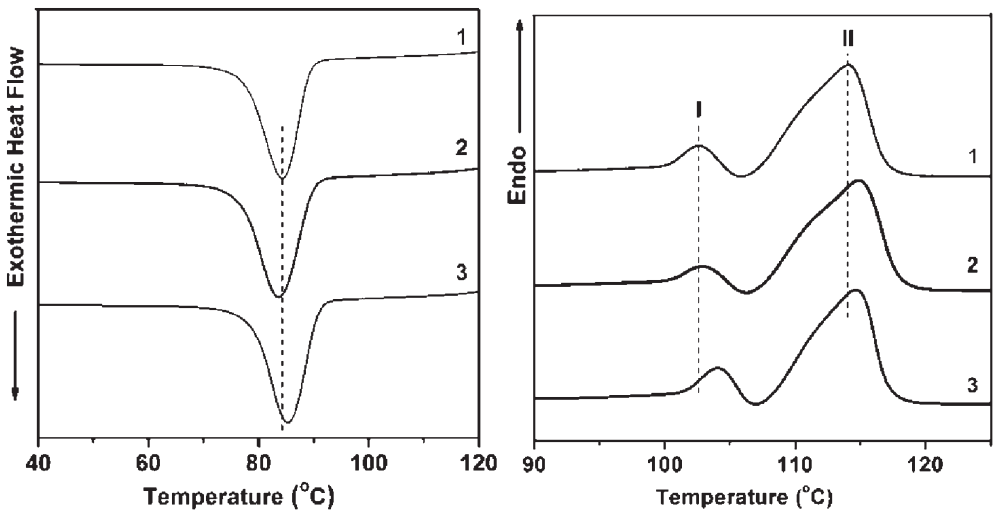


**Figure 8.** Cooling (left) and second heating (right) DSC curves of pristine PBS (curve 1), MWCNTs/PBS physical mixture (curve 2) and PBS-*g*-MWCNTs (curve 3) (translated curves).

cooling and second heating scans of PBS, PBS-*g*-MWCNTs and MWCNTs/PBS samples are shown in Fig. 8, and the related thermal data are reported in Table 3.

The glass transition temperature ($T_g$) of the samples was determined by DSC on the second heating scan. The $T_g$ of PBS slightly increases with the incorporation of MWCNTs, irrespective of grafting or physical mixing. This means that the nanotubes slightly altered the mobility of the small portions of chain responsible for the glass transition. A single exothermic peak was observed for each sample during the cooling process. The crystallization temperature ($T_c$) of the PBS-*g*-MWCNTs sample was higher than that of the physical blend probably indicating that a slight nucleating action occurred. This result might reflect a better dispersion of the MWCNTs chemically immobilized to the PBS compared to the bare particles simply dispersed in the matrix. Finally, two endothermic melting peaks were observed for all the samples during the second heating scan. This effect is due to the coexistence of two main populations of crystals with

**Table 3.** DSC parameters of neat PBS, MWCNTs/PBS and PBS-*g*-MWCNTs

| | DSC data | | | | |
|---|---|---|---|---|---|
| Sample | $T_g$ (°C) | $T_c$ (°C) | $\Delta H_c$ (J g$^{-1}$) | $T_m$I/$T_m$II (°C) | $\Delta H_m$ (J g$^{-1}$) |
| PBS | −32.6 ± 0.4 | 84.3 ± 0.3 | 76.5 ± 1.1 | 102.6 ± 0.7/114.1 ± 0.4 | −75.8 ± 2.5 |
| MWCNTs/PBS | −30.6 ± 0.6 | 83.6 ± 0.4 | 84.4 ± 2.3 | 102.9 ± 0.5/114.9 ± 0.4 | −83.2 ± 2.7 |
| PBS-*g*-MWCNTs | −31.6 ± 0.6 | 85.2 ± 0.3 | 83.2 ± 2.1 | 104.1 ± 0.6/114.7 ± 0.5 | −80.7 ± 2.0 |

$T_g$ is the glass transition temperature of PBS registered during the second heating scan; $T_c$ is the crystallization temperature of PBS registered during the cooling; $T_m$I and $T_m$II are the two melting peaks observed during the second heating scan; $\Delta H_m$ is the melting enthalpy. $T_m$I and $T_m$II, $\Delta H_c$ and $\Delta H_m$ are mean values of three measurements ± standard deviation.

different thicknesses and, as a consequence, with different melting temperatures ($T_m$I melting temperature of thinner lamellas, $T_m$II melting temperature of thicker crystals).[16,40] Moreover, a weak recrystallization peak between the two endothermic peaks can be observed (Fig. 8), which has been ascribed to the recrystallization during the heating scan of the defective crystals (fraction of thinner lamellas).[40–42] Neither $T_m$II nor the melting enthalpy $\Delta H_m$ change significantly in the presence of the nanotubes. Differently, $T_m$ I is higher in the presence of PBS-grafted nanotubes, which confirms that they are effective in promoting the nucleation of stable thin crystallites.[16] Again, as inferred from rheological analyses, a better nanotube dispersion can be assumed in the PBS-*g*-MWCNTs sample.

## CONCLUSIONS

TEMPO functionalized MWCNTs were prepared by the Cu(I)-catalyzed azide/alkyne click chemistry reaction and later PBS polymer chains were grafted to the surface of MWCNTs-*g*-TEMPO via NRC. This method was successful in promoting the grafting of PBS chains on the sidewalls of MWCNTs thus demonstrating the feasibility of the NRC reaction as a 'grafting to' method. The presence of TEMPO radicals on the functionalized MWCNTs and the grafting of PBS to the surface of MWCNTs were confirmed by EPR and ATR-FTIR analyses. The longer correlation time of nitroxide moieties grafted on MWCNTs with respect to that of free nitroxide demonstrated the confinement via chemical bonding of the nitroxide motions. A partial detachment of the polymer chains from the PBS-*g*-MWCNTs system was obtained by thermal treatment at 180 °C in the EPR cavity via homolytic cleavage of the C – ON bond with the concomitant appearance of the three-line nitroxide signal.

Compared with the physical mixture of PBS and MWCNTs, the PBS-*g*-MWCNTs improved dispersion and promoted interaction within the polymer matrix as supported by DSC and rheology measurements. Rheological analyses indicated that both the PBS-*g*-MWCNTs and MWCNT/PBS samples are above the filler percolation threshold, but the filler network based on the PBS-grafted nanotubes is much more robust than that based on bare nanotubes. This was ascribed to a better quality of stress transfer across the polymer – filler interface and, probably, to a higher degree of dispersion of the PBS-grafted nanotubes. The latter hypothesis seemed to be supported by DSC investigations, which also proved a moderate nucleating ability of the functionalized nanotubes.

On the whole, the results demonstrate that this protocol allows the immobilization of MWCNTs in the PBS polymer with advantages in the morphological and final properties of the composite material.

## ACKNOWLEDGEMENTS

This work was supported by MIUR under the program FIRB 2010-Futuro in Ricerca, project title 'GREENER – Towards multifunctional, efficient, safe and stable "green" bio-plastics based nanocomposites of technological interest via the immobilization of functionalized nanoparticles and stabilizing molecules' (Project code: RBFR10DCS7). We wish to thank Dr G. Nasillo (Centro Grandi Apparecchiature – UninetLab, University of Palermo) for the TEM analysis. G. F. thanks Dr Giuliana Stabile for the support in rheological analyses and TGA. Dr Carlo Punta and Ing. Lucio Melone (Politecnico di Milano) are kindly acknowledged for their technical suggestions about the click reaction.

## SUPPORTING INFORMATION

Supporting information may be found in the online version of this article.

## REFERENCES

1 Lim ST, Hyun YH, Choi HJ and Jhon MS, *Chem Mater* **14**:1839–1844 (2002).
2 Li H, Chang J, Cao A and Wang J, *Macromol Biosci* **5**:433–440 (2005).
3 Fujimaki T, *Polym Degrad Stab* **59**:209–214 (1998).
4 Tasis D, Tagmatarchis N, Bianco A and Prato M, *Chem Rev* **106**:1105–1136 (2006).
5 Beyou E, Akbar S, Chaumont P and Cassagnau P, Polymer nanocomposites containing functionalised multiwalled carbon nanotubes, in *Syntheses and Applications of Carbon Nanotubes and Their Composites*, ed. by Suzuki S. InTech, pp. 77–115 (2013).
6 Pramoda KP, Linh NTT, Zhang C and Liu T, *J Appl Polym Sci* **111**:2938–2945 (2009).
7 Shih YF, Chen LS and Jeng RJ, *Polymer* **49**:4602–4611 (2008).
8 Wang G, Guo B, Xu J and Li R, *J Appl Polym Sci* **121**:59–67 (2011).
9 Yuan L, Wu D, Zhang M, Zhou W and Lin D, *Ind Eng Chem Res* **50**:14186–14192 (2011).
10 Ali FB and Mohan R, *Polym Comp* **31**:1309–1314 (2010).
11 Song L and Qiu Z, *Polym Adv Technol* **22**:1642–1649 (2011).
12 Lim SK, Lee SI, Jang SG, Lee KH, Choi HJ and Chin IJ, J Macromol Sci *B Phys* **50**:1171–1184 (2011).
13 Song L and Qiu Z, *Polym Degrad Stab* **94**:632–637 (2009).
14 Shih YF, J Polym Sci *B Polym Phys* **47**:1231–1293 (2009).
15 Lin CS, Shih YF, Jeng RJ, Dai SA, Lin JJ and Lee CC, *J Taiwan Inst Chem Eng* **43**:322–328 (2012).
16 Tan L, Chen Y, Zhou W, Ye S and Wei J, *Polymer* **52**:3587–3596 (2011).
17 Spitalsky Z, Tasis D, Papegelis K and Galiotis C, *Prog Polym Sci* **35**:357–401 (2010).
18 Baskran D, Mays JW and Bratcher MS, *Angew Chem Int Ed* **43**:2138–2142 (2004).
19 Chen GX, Kim HS, Park BH and Yoon JS, *Macromol Chem Phys* **208**:389–398 (2007).
20 Song W, Zheng Z, Tang W and Wang X, *Polymer* **48**:3658–3663 (2007).
21 Cicogna F, Coiai S, Passaglia E, Tucci I, Ricci L, Ciardelli F et al., *J Polym Sci A Polym Chem* **49**:781–795 (2011).
22 Cicogna F, Coiai S, Pinzino C, Ciardelli F and Passaglia E, *React Funct Polym* **72**:695–702 (2012).
23 Cicogna F, Coiai S, Rizzarelli P, Carroccio S, Gambarotti C, Domenichelli I et al., *Polym Chem* **5**:5656–5667 (2014).
24 Fan DQ, He JP, Tang W, Xu JT and Yang YL, *Eur Polym J* **43**:26–34 (2007).
25 Kolb HC, Finn MG and Sharpless KB, *Angew Chem Int Ed* **40**:2004–2021 (2001).
26 Moses JE and Moorhouse AD, *Chem Soc Rev* **36**:1249–1262 (2007).
27 Harris PJF, *Carbon Nanotube Science Synthesis, Properties and Applications*. Cambridge University Press, New York (2009).
28 Peng H, Alemany LB, Margrave JL and Khabashesku VN, *J Am Chem Soc* **125**:15174–15182 (2003).
29 Boudalis AK, Policand X and Sournia A, *Inorg Chim Acta* **361**:1681–1688 (2008).
30 Gheorghe A, Matsuno A and Reiser O, *Adv Synth Catal* **348**:1016–1020 (2006).
31 Romanova EE, Akiel R, Cho FH and Takahashi S, *J Phys Chem A* **117**:11933–11939 (2013).
32 Su X, Shuai Y, Guo Z and Feng Y, *Molecules* **18**:4599–4612 (2013).
33 Ambrosetti R and Ricci D, *Rev Sci Instrum* **62**:2281–2287 (1991).
34 Pinzino C, Forte C, EPR_ENDOR, ICQEM-CNR, Rome (1992).
35 Zaremski MY, Plutalova AV, Garina ES, Lachinov MB and Golubev VB, *Macromolecules* **32**:6359–6362 (1999).
36 Stipa P, Greci L, Carloni P and Damiani E, *Polym Degrad Stab* **55**:323–327 (1997).
37 Studer A, *Chem Soc Rev* **33**:267–273 (2004).
38 Tseng CH, Wang CC and Chen CY, *Chem Mater* **19**:308–315 (2007).
39 Kim HS, Park BY, Yoon JS and Jin HJ, *Eur Polym J* **43**:1729–1735 (2007).
40 Yasuniwa M and Satou T, *J Polym Sci B Polym Phys* **40**:2411–2420 (2002).
41 Yoo ES and Im SS, J Polym Sci *B Polym Phys* **37**:1357–1366 (1999).
42 Yasuniwa M, Tsubakihara S, Satou T and Iura K, *J Polym Sci B Polym Phys* **43**:2039–2047 (2005).